JOURNAL OF AIRCRAFT
Vol. 34, No. 3, May–June 1997

Gradient-Based Aerodynamic Shape Optimization Using Alternating Direction Implicit Method

Mohagna J. Pandya* and Oktay Baysal†
Old Dominion University, Norfolk, Virginia 23529-0247

A gradient-based shape optimization methodology that is intended for practical three-dimensional aerodynamic applications has been developed. It is based on the quasianalytical sensitivities. The flow analysis is rendered by a fully implicit, finite volume formulation of the Euler equations. The aerodynamic sensitivity equation is solved using the alternating direction implicit algorithm for memory efficiency. A flexible wing geometry model that is based on surface parameterization and planform schedules is utilized. The present methodology and its components have been tested via several comparisons. Initially, the flow analysis for a wing is compared with those obtained using an unfactored, preconditioned conjugate gradient approach (PCG) and an extensively validated computational fluid dynamics code. Then, the sensitivities computed with the present method have been compared with those obtained using the finite difference and PCG approaches. Effects of grid refinement and convergence tolerance on the analyses and the shape optimization have been explored. Finally, the new procedure has been demonstrated in the design of a cranked arrow wing at Mach 2.4. Despite the expected increase in the computational time, the results indicate that shape optimization problems, which require large numbers of grid points, can be resolved with a gradient-based approach.

Nomenclature

A	= area of airfoil section
AOA	= angle of attack
C_D	= coefficient of drag
C_L	= coefficient of lift
C_L/C_D	= lift-to-drag ratio
C_P	= coefficient of pressure
c, chd, chdscal	= chord and its distribution
$\boldsymbol{D}$	= design variables
$\boldsymbol{F}$	= objective function
$\hat{\boldsymbol{F}}$, $\hat{\boldsymbol{G}}$, $\hat{\boldsymbol{H}}$	= fluxes in curvilinear coordinates
$\boldsymbol{G}$	= constraints
$\boldsymbol{M}$	= vector of metric terms
NDV	= number of design variables
$\boldsymbol{Q}$	= vector of conserved flow variables
$\boldsymbol{Q}'$	= sensitivity of Q to design variable
$\boldsymbol{R}$	= residual
s	= arc length
spn	= half-span length
t, thk, thkscal	= thickness and its distribution
tranx, tranz	= coordinates of wing leading edge
twst	= geometric twist
V	= wing volume
$\boldsymbol{X}$	= vector of volume-grid coordinates
$\boldsymbol{\Delta Q}$	= correction to flow variables
ε	= tolerance
θ	= included angle at trailing edge
Λ	= sweep angle
$\boldsymbol{\lambda}$	= adjoint-variable vector
ω	= relaxation parameter

Subscripts

b	= body surface
crank	= mid-half-span location
LE	= wing leading edge
TE	= wing trailing edge

Superscript

n	= time level

Special Symbol

$\boldsymbol{\nabla F}$	= gradient of objective function

Introduction

DEVELOPING an effective three-dimensional design optimization procedure, which is also automated and practical to use, has been a topic of intense research since its introduction two decades ago.[1] Despite the formidable strides made in recent years, the challenge does not appear to have been met.

The accuracy of a gradient-based optimization method, and the efficiency with which it can accomplish this, are directly related to the accurate and efficient receipt of the gradient information on the objectives and the constraints. These sensitivity coefficients can be delivered to the optimizer via sensitivity analysis, which often refers to the quasianalytically obtained sensitivities, rather than those obtained by the traditional finite differences approach. To this end, the governing equations of fluid flow can be differentiated analytically either starting with their original differential form and using the variational concepts[2,3] (variational sensitivity analysis; also known as continuous method, adjoint formulation, or control theory approach), or after they have been discretized[4] (discrete sensitivity analysis).

In the variational sensitivity analysis approach, the co-state equations (or the adjoint equations) are partial differential equations, which are of the same order and character as the flow equations. Hence, they can be discretized and solved for the perturbations of the dependent variables by the same computational fluid dynamics (CFD) technique, resulting in its computer memory requirement being no more than what the flow analysis requires.[5] Nonetheless, this approach is not without a drawback: its analytical development is highly case de-

Presented as Paper 96-0091 at the AIAA 34th Aerospace Sciences Meeting, Reno, NV, Jan. 15–18, 1996; received March 16, 1996; revision received Jan. 21, 1997; accepted for publication Jan. 22, 1997.

*Graduate Research Assistant, Aerospace Engineering Department. Student Member AIAA.

†Professor and Eminent Scholar, Aerospace Engineering Department. Associate Fellow AIAA.

pendent, rather cumbersome, and may be characterized as front-end loaded.

Since the early 1990s, there have been promising developments in aerodynamic design optimization based on discrete sensitivity analysis.[6] Its computational-time efficiency has been addressed in several ways,[7] including the surface parameterization using Bezier splines and Bernstein polynomials, and solving the unfactored CFD equations by a quasi-Newton method. The computer storage efficiency was later addressed, first by examining the solution of all the equations using a preconditioned conjugate gradient (PCG) method,[8] then by the multiblock sensitivity analysis scheme.[9] An important benefit of the multiblock sensitivity analysis scheme was its applicability to a complex and multicomponent geometry, around which structured grids could only be generated by the use of domain decomposition techniques. The multiblock sensitivity analysis was extended for three-dimensional shapes, where a PCG method was also incorporated[10] and applied in the optimization of a multiple-component configuration.[11]

In the PCG methods previously mentioned,[8,10] incomplete lower–upper (ILU) decompositions of the coefficient matrix with some fill-in [ILU(n), $n > 0$] were used for the preconditioning. Another preconditioning option is to use the approximate factors of the coefficient matrix, then break the problem into a sequence of simpler problems; that is the premise of the alternating direction implicit (ADI) schemes, which have been used to solve the CFD equation for more than two decades.[12] The tradeoff in the latter approach is a slower convergence for the much reduced computer memory storage.[13]

The results from all of the applications just cited indicate that, in general, the design methods obtain a final shape via an evolution of successively improved shapes. A practical use of fully implicit CFD methods (quasi-Newton method) within an optimization procedure allows the realization of high convergence rates and a consequent reduction of CPU time. The memory requirement of such a procedure that uses a PCG algorithm is low as compared to direct inversion solvers. However, this memory requirement is high enough to preclude the realistic, high-grid–density design of a practical three-dimensional geometry such as a wing or wing–body combination.

This particular limitation served as the impetus to improve upon the recently developed three-dimensional optimization methodology, which was demonstrated for a transport wing,[14] and later it was applied for shaping asymmetric delta wings and cranked delta wings.[15] This improvement has been achieved by the use of ADI-factored operators to serve as preconditioning matrices for the CFD as well as the sensitivity equations.

Synopsis of Methodology

Aerodynamic design optimization aims at the extremization of an objective function $\boldsymbol{F}[\boldsymbol{D}, \boldsymbol{Q}(\boldsymbol{D})]$ subject to constraints $\boldsymbol{G}[\boldsymbol{D}, \boldsymbol{Q}(\boldsymbol{D})]$. Both F and G may be nonlinear or nonsmooth[16] functions of D and Q. In the present formulation, F and G are obtained from the governing equations of three-dimensional, compressible, inviscid flow, which are written in the steady-state residual form

$$\boldsymbol{R} = \boldsymbol{R}\{\boldsymbol{Q}(\boldsymbol{D}), \boldsymbol{M}[\boldsymbol{X}(\boldsymbol{D})]\} = \vartheta(\varepsilon) \tag{1}$$

Their fully implicit discretization written in delta, or deficit correction, form is

$$\left(\frac{\partial \boldsymbol{R}}{\partial \boldsymbol{Q}}\right)^n \boldsymbol{\Delta Q}^n = -\boldsymbol{R}(\boldsymbol{Q}^n, \boldsymbol{M}) \tag{2}$$

Equation (2) was discretized in space using a cell-centered, control-volume formulation. The flux vectors and the Jacobian matrix $\partial R/\partial Q$ were evaluated using the flux-vector-splitting technique of van Leer. The cell interface values of Q were

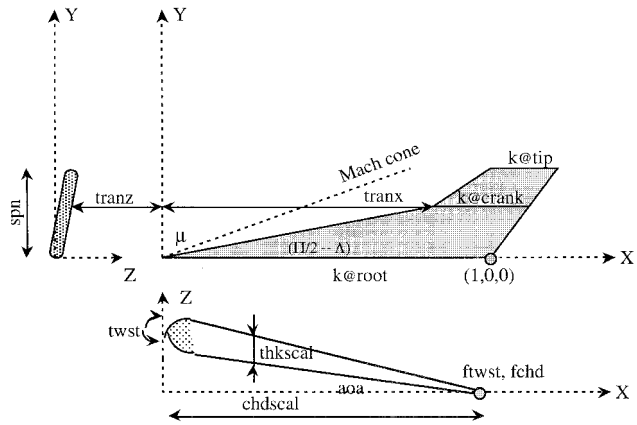

Fig. 1 Parameterization of a wing.

determined using a spatially third-order accurate, upwind-biased, MUSCL interpolation formula with a van Albada flux limiter.

A strict application of Newton method, including consistent treatment of the boundary conditions, generally results in very large error reductions per iteration; quadratic convergence is achieved when the solution enters the domain of attraction to the root. However, because of the large memory requirement of the method, practical application of the same is thwarted. Since at convergence the deficit correction is within $\vartheta(\varepsilon)$, the coefficient matrix in Eq. (2) is simply a preconditioner for an iterative method. Even then, the memory storage required for a large-size problem is rather prohibitive.[8,10] In the present work, this is circumvented by resorting to a first-degree iterative scheme, where the true Jacobian matrix is split into more memory-manageable parts using the approximate factorization followed by the ADI scheme.[12]

The employed optimization algorithm is based on the method of feasible directions, which is coded in ADS.[17] This method requires the first-order sensitivity gradients of both the objective function and the constraints. In the present formulation, these gradients are evaluated analytically. The analytic gradient of, for example, the objective function (similarly, it can be written for the constraints) is expressed by

$$\boldsymbol{\nabla F} = \frac{\partial \boldsymbol{F}(\boldsymbol{D}, \boldsymbol{Q})}{\partial \boldsymbol{D}_i}\,\hat{\boldsymbol{e}}_i = \left[\left(\frac{\partial \boldsymbol{F}}{\partial \boldsymbol{D}_i}\right)_{\boldsymbol{Q}} + \left(\frac{\partial \boldsymbol{F}}{\partial \boldsymbol{Q}}\right)_{\boldsymbol{D}}^{T} \boldsymbol{Q}_i'\right] \hat{\boldsymbol{e}}_i \qquad i \in \{1, \ldots, \mathrm{NDV}\} \tag{3}$$

where $\boldsymbol{Q}_i' \equiv \partial \boldsymbol{Q}/\partial \boldsymbol{D}_i$.

For the discrete sensitivity analysis, either the direct method or the adjoint-variable method,[4–7] given next, respectively, is used:

$$\left(\frac{\partial \boldsymbol{R}}{\partial \boldsymbol{Q}}\right)_{\boldsymbol{D}} \boldsymbol{Q}' = -\left(\frac{\partial \boldsymbol{R}}{\partial \boldsymbol{D}}\right)_{\boldsymbol{Q}} \tag{4}$$

$$\left(\frac{\partial \boldsymbol{R}}{\partial \boldsymbol{Q}}\right)_{\boldsymbol{D}}^{T} \boldsymbol{\lambda}_F = \left(\frac{\partial F}{\partial Q}\right)_{\boldsymbol{D}} \tag{5}$$

The direct formulation renders $\boldsymbol{Q}'$ explicitly, which allows the use of approximate flow analyses,[6] but the number of equations to be solved scales with the number of design variables. The number of equations to be solved in the adjoint formulation, however, scales with the number of aerodynamic constraints plus one for the objective.

Following the same solution options considered for the analysis equation, Eq. (1), the sensitivity equation, Eq. (4) or (5), is written in the delta form as shown next, respectively,

$$\left(\frac{\partial \hat{\boldsymbol{R}}}{\partial \boldsymbol{Q}}\right)_{\boldsymbol{D}}^{n} \{\Delta \boldsymbol{Q}'\}^n = -\left(\frac{\partial \boldsymbol{R}}{\partial \boldsymbol{Q}}\right)_{\boldsymbol{D}}^{n} Q'^n - \left(\frac{\partial \boldsymbol{R}}{\partial \boldsymbol{D}}\right)_{\boldsymbol{Q}} \tag{6}$$

Table 1 Geometry of initial arrow wing

Λ_{LE} and Λ_{TE}, deg	Aspect ratio	$(t/c)_{root,mid,tip}$, %	θ_{tip}, deg	Half-span/c_{root}
72 – 56.3	1.01	4.80, 4.55, 4.80	6.80	0.57

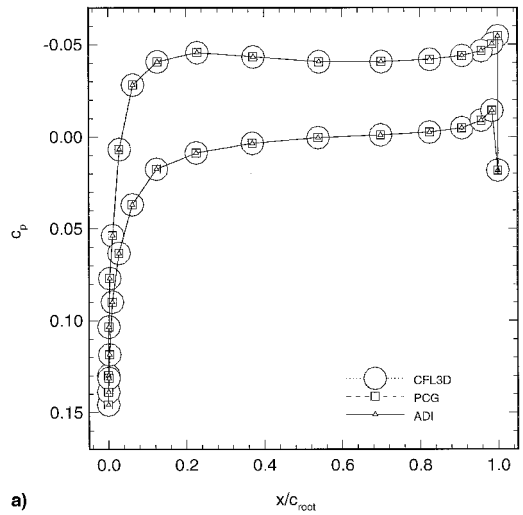

a)

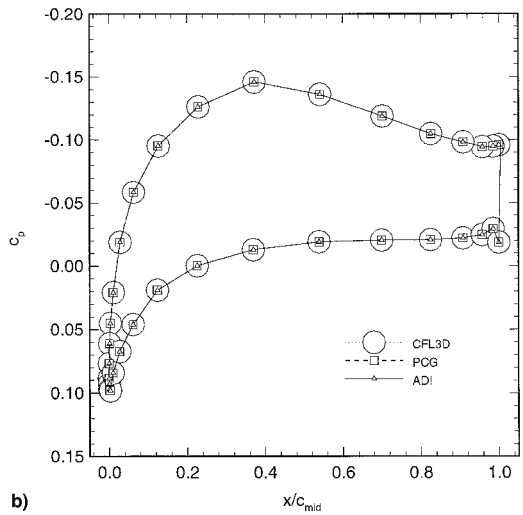

b)

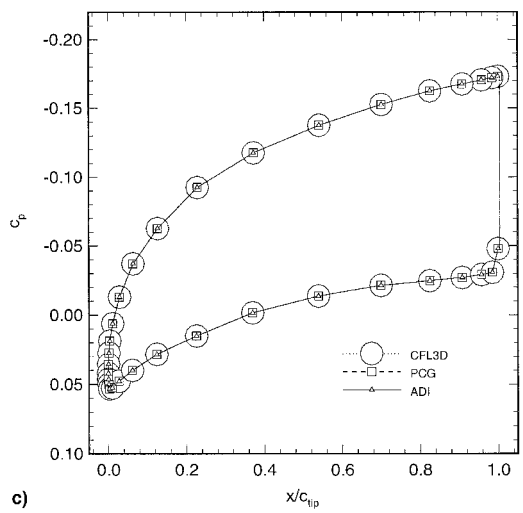

c)

Fig. 2 Comparison of chordwise pressure coefficients on coarse grid (43 × 15 × 9): a) root section, b) midsection, and c) tip section. $M_\infty = 2.4$, AOA = 3 deg.

Table 2 Efficiency and accuracy comparisons for CFD analyses[a]

	PCG	ADI	
	Coarse grid, 43 × 15 × 9[b]	Coarse grid, 43 × 15 × 9	Fine grid, 127 × 43 × 25
Iterations to convergence	100	241	327
CPU time, s	640[c]	283	8138
Memory, MWord	10.61	2.25	42.11
C_L	8.4815e-02	8.4814e-02	8.7349e-02
C_D	7.8270e-03	7.8270e-03	7.6629e-03
C_L/C_D	10.8362	10.8362	11.40

[a]Computed flowfield for $M_\infty = 2.4$.
[b]In circumferential, normal, and spanwise directions, respectively.
[c]Initialized with converged ADI solution of $M_\infty = 2.35$ flow.

$$\left(\frac{\partial \hat{\boldsymbol{R}}}{\partial \boldsymbol{Q}}\right)^T \{\Delta \boldsymbol{\lambda}_F\}^n = -\left(\frac{\partial \boldsymbol{R}}{\partial \boldsymbol{Q}}\right)_D^T \{\boldsymbol{\lambda}_F\}^n - \left(\frac{\partial \boldsymbol{F}}{\partial \boldsymbol{Q}}\right)_D \tag{7}$$

Here, $\partial \hat{\boldsymbol{R}}/\partial \boldsymbol{Q}$ is an approximation to the true Jacobian that is used as a preconditioner. Note that the delta form of the adjoint equation for the constraints can be written similar to Eq. (7). Then, these equations are either solved using the PCG approach, or they are approximately factored, then solved by the ADI scheme. With the addition of a relaxation term for diagonal dominance, the ADI scheme is written as

$$\begin{aligned}\left(\frac{\boldsymbol{I}}{\omega} + \frac{\partial \hat{\boldsymbol{F}}}{\partial \boldsymbol{Q}}\right)^n \Delta \boldsymbol{Q}'^* &= -\left(\frac{\partial \boldsymbol{R}}{\partial \boldsymbol{Q}}\right)_D^n \boldsymbol{Q}'^n - \left(\frac{\partial \boldsymbol{R}}{\partial \boldsymbol{D}}\right)_Q \\ \left(\frac{\boldsymbol{I}}{\omega} + \frac{\partial \hat{\boldsymbol{G}}}{\partial \boldsymbol{Q}}\right)^n \Delta \boldsymbol{Q}'^{**} &= \left(\frac{\boldsymbol{I}}{\omega}\right) \Delta \boldsymbol{Q}'^* \\ \left(\frac{\boldsymbol{I}}{\omega} + \frac{\partial \hat{\boldsymbol{H}}}{\partial \boldsymbol{Q}}\right)^n \{\Delta \boldsymbol{Q}'\}^n &= \left(\frac{\boldsymbol{I}}{\omega}\right) \Delta \boldsymbol{Q}'^{**}\end{aligned} \tag{8}$$

ω may be set to $\Delta\tau$, where τ is a time-like variable, or other conventional options may be used.[14] For simplicity, the coefficient matrices in Eq. (8) are constructed using the first-order-accurate upwind scheme, and the consistent linearization of the boundary conditions is neglected.

The wing geometry used for demonstration herein is generated using the parameterization adopted from Burgreen and Baysal.[14] This wing is generated from the geometrically simple wing that is unswept, untwisted, uncambered, and rectangular, with both its chord and span equal to unity; hence, this wing is referred to as the unit wing. To generate a variety of shapes, the geometric parameterization of a wing should allow flexibility in its sections, taper distribution, sweep, span, spanwise bending, geometric twist, and global angle of attack. In the present parameterization (Fig. 1), each feature is implemented as an independent geometric operation in a sequential manner. Its details can be found from Burgreen and Baysal.[14]

Once a new wing shape and its surface grid are defined, the next task is the regeneration of its volume grid. This process of regridding enroute to the optimized shape is completed using the flexible grid approach,[14] where the volume grid is written as a function of the body surface grid X_b. As the surface is changed during the shape optimization, the x coordinates, for example, of the new volume grid are found using the following relations:

$$x_i^{new} = x_i^{old} + [1 - V_j](x_b^{new} - x_b^{old}) \tag{9a}$$

where

$$V_j = \frac{s_j - s_2}{s_{j\max} - s_2} \tag{9b}$$

$$s_j = \sum_{i=2}^{j} \sqrt{(x_i - x_{i-1})^2 + (y_i - y_{i-1})^2 + (z_i - z_{i-1})^2} \tag{9c}$$

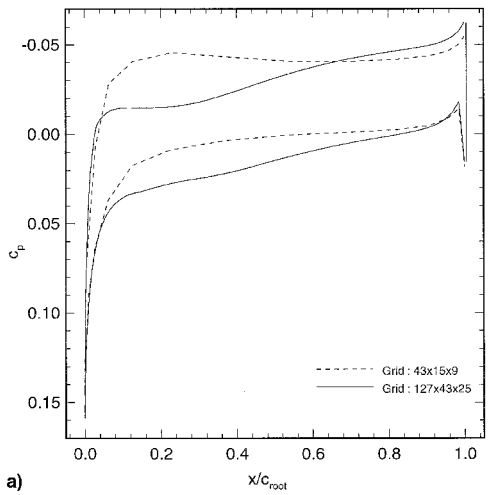

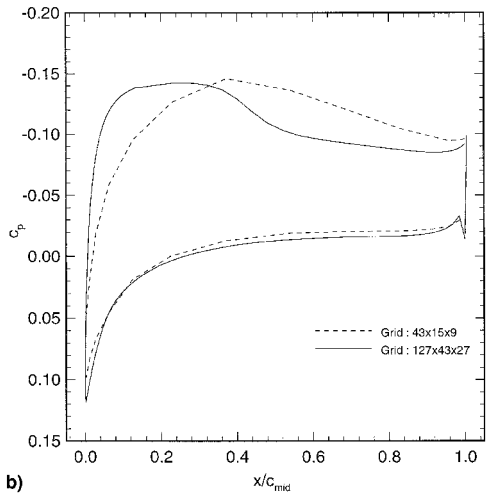

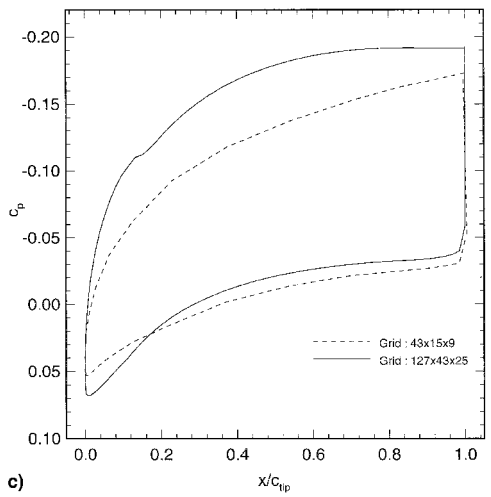

Fig. 3 Comparison of chordwise pressure coefficients by the ADI method on fine and coarse grids: a) root section, b) midsection, and c) tip section. M_∞ = 2.4, AOA = 3 deg.

Results

Validation of ADI Approach

To test the presently developed ADI methodology, an arrow wing (Table 1) was considered to be at 3-deg AOA to an oncoming Mach 2.4 flow. This wing was generated from the unit wing by linear distributions of `chdscal` and `thkscal` along the span as schematically shown in Fig. 1. The entire wing was behind the Mach cone. The coarse grid was used to accommodate the memory-intensive PCG solutions within reasonable computer resources, as well as for the grid refinement studies.

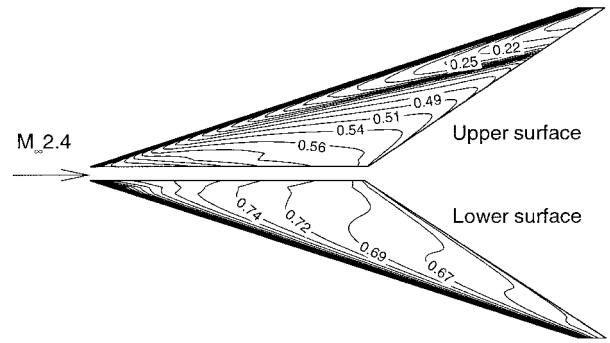

Fig. 4 Normalized pressure contours by ADI method on fine grid (127 × 43 × 25). M_∞ = 2.4, AOA = 3 deg.

The flowfield was computed on the coarse grid using the present ADI and PCG methods as well as CFL3D[18] (Version 3.0). The results of these analyses were successfully compared (Fig. 2) via their chordwise pressure coefficient distributions at three spanwise sections. The drag values of CFL3D and ADI (7.6e-3 vs 7.8e-3) matched to the third digit and, for the ADI and PCG solutions, the lift and drag values matched up to five significant digits (Table 2).

As it is necessary for quasi-Newton methods, the PCG method was initialized with the solution to a M_∞ = 2.35 flow, obtained using the ADI method. Then, the convergence to the M_∞ = 2.4 solution was timed for both of the methods (Table 2). As expected, by using ADI, the storage was reduced by a factor of about 6 compared to the PCG, even for this coarse grid. The initialization, apparently, was not in the domain of attraction to the root, hence, the convergence time of PCG was also unexpectedly higher.

In Fig. 3, the chordwise pressure coefficient distributions, obtained on the coarse and fine grids with the ADI method, are presented for three sections. Although the coarse-grid flowfield appeared plausible with its salient features, improvement in the solution because of grid refinement was clearly observed: with coarse-grid computations, the pressure peaks were overestimated in the root section, yet they were underestimated in the mid and tip sections. The surface pressures obtained on the fine grid (Fig. 4) were deemed satisfactory based on the general flowfield features, such as, the crisper definition of the upper surface shock. More conclusive evidence to an almost grid-independent solution, however, would have required another level of finer grid solution that would differ only insignificantly, if at all, from the current fine-grid solution.

Next, the sensitivities were computed by the PCG and ADI methods using the direct differentiation [Eqs. (4) and (8)] on the coarse grid. The primary reason for the computations on the coarse grid was naturally the significant cost savings. Note that the point of this exercise was a fair comparison of the sensitivities from different methods, and not their absolute accuracy. Most of the values matched to the fourth significant digit (Table 3). As for the efficiencies, this comparison essentially epitomized the characteristics of both the methods. The unfactored solution procedure based on PCG method, when in the domain of attraction to its root, was very efficient from the CPU time standpoint. Whereas, the factored solution procedure (ADI) could only achieve the linear convergence, but it was very efficient from the memory viewpoint. The results shown in Table 3 were obtained using a convergence criterion of five orders of magnitude reduction in the L_2-norm residual. Because this much reduction may not always be necessary during an optimization, the effect of the order of magnitude on the efficiency and accuracy was investigated (Table 4). Each two orders of reduction increased the CPU time by a factor of about 1.6. Generally, the change in the values, when the resid-

ual was dropped from five orders to seven orders, was in the fifth or higher significant digit. Finally, ADI-based sensitivities, obtained for the convergence criterion of three orders of reduction, were compared with those by the finite difference method[4,6] and they were found to be in excellent agreement (Table 5).

Shape Optimization

The primary thrust of the present study was to apply the gradient-based optimization technique for three-dimensional shapes, which often require large size grids. The challenge was to perform such a task using only a feasible amount of computer memory, despite the fact that higher grid densities than what has been used previously[14,15] were needed. As a demonstration, the present method was implemented to optimize a supersonic arrow wing configuration (Table 1 and Fig. 4), first on a coarse grid and then on a fine grid.

The present problem formulation had nine design variables (spn, and at mid and tip sections: thkscal, chdscal, tranx, and twst). The objective function was selected to be

Table 3 Comparison of quasianalytical sensitivities[a]

	ADI	PCG
Iterations to convergence	112	9
CPU time, s	344	45
Memory, MWord	2.60	10.61
$\frac{\partial C_L}{\partial(\mathrm{chd}_{tip})}$	0.0217	0.0217
$\frac{\partial C_L}{\partial(\mathrm{tranx}_{mid})}$[b]	−0.0142	−0.0142
$\frac{\partial C_L}{\partial(\mathrm{spn})}$	0.0439	0.0439
$\frac{\partial(C_L/C_D)}{\partial(\mathrm{tranx}_{mid})}$	2.5124	2.5120
$\frac{\partial(C_L/C_D)}{\partial(\mathrm{tranx}_{tip})}$	2.7549	2.7549
$\frac{\partial(C_L/C_D)}{\partial(\mathrm{spn})}$	−10.4890	−10.4881

[a]Computed flowfield for $M_\infty = 2.4$ on 43 × 15 × 9 C–H grid; direct method [Eqs. (4) and (8)] with $\vartheta(5)$ convergence.
[b]Parameters as defined in Fig. 1.

Table 4 Effect of convergence tolerance on efficiency and accuracy of sensitivities for ADI method[a]

	$\vartheta(3)$	$\vartheta(5)$	$\vartheta(7)$
Iterations to convergence	65	112	163
CPU time, s	204	344	498
$\frac{\partial C_L}{\partial(\mathrm{chd}_{tip})}$	0.0217	0.0217	0.0217
$\frac{\partial C_L}{\partial(\mathrm{tranx}_{mid})}$	−0.0142	−0.0142	−0.0142
$\frac{\partial C_L}{\partial(\mathrm{spn})}$	0.0439	0.0439	0.0439
$\frac{\partial(C_L/C_D)}{\partial(\mathrm{chd}_{mid})}$	7.0183	7.0186	7.0186
$\frac{\partial(C_L/C_D)}{\partial(\mathrm{tranx}_{mid})}$	2.5128	2.5124	2.5124
$\frac{\partial(C_L/C_D)}{\partial(\mathrm{tranx}_{tip})}$	2.7547	2.7549	2.7549
$\frac{\partial(C_L/C_D)}{\partial(\mathrm{spn})}$	−10.4889	−10.4890	−10.4890

[a]Computed flowfield for $M_\infty = 2.4$ on 43 × 15 × 9 C–H grid; direct method [Eq. (8)].

Table 5 Comparison of ADI (quasianalytical) and finite difference sensitivities[a]

	Quasianalytical[b]	Finite difference	Quasianalytical/ finite difference
$\frac{\partial C_L}{\partial(\mathrm{chd}_{tip})}$	0.0217	0.0216	1.0055
$\frac{\partial C_L}{\partial(\mathrm{twst}_{crank})}$	0.0124	0.0124	0.9993
$\frac{\partial C_D}{\partial(\mathrm{thk}_{tip})}$	0.0007	0.0007	0.9956
$\frac{\partial C_D}{\partial(\mathrm{tranx}_{crank})}$	−0.0031	−0.0031	1.0006
$\frac{\partial C_D}{\partial(\mathrm{twst}_{crank})}$	0.0014	0.0014	1.0005
$\frac{\partial(C_L/C_D)}{\partial(\mathrm{chd}_{tip})}$	2.3543	2.3571	0.9988
$\frac{\partial(C_L/C_D)}{\partial(\mathrm{twst}_{crank})}$	−0.4108	−0.4091	1.0065
$\frac{\partial(C_L/C_D)}{\partial(\mathrm{spn})}$	−10.4889	−10.4829	1.0006

[a]Computed flowfield for $M_\infty = 2.4$ on 43 × 15 × 9 C–H grid.
[b]Direct method [Eq. (8)] with $\vartheta(3)$ convergence.

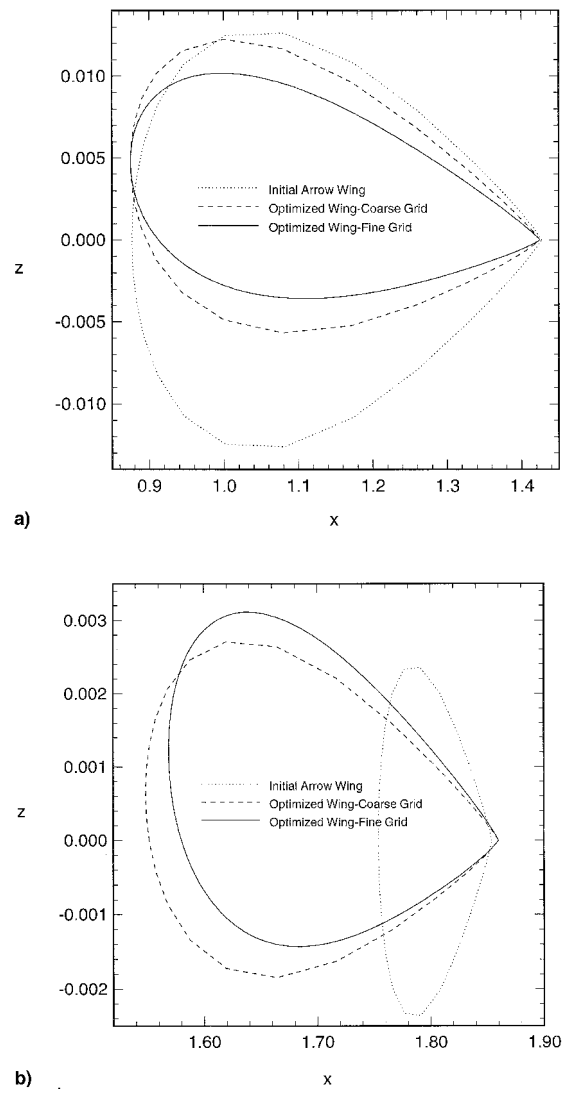

Fig. 5 Evolution of wing sections from initial to coarse- and fine-grid optimized shapes: a) midsection and b) tip section airfoils.

Table 6 Aerodynamics and geometry of optimized wing

	Coarse grid, 43 × 15 × 9	Fine grid, 127 × 43 × 25
C_L	9.5675e-02	9.9113e-02
C_D	7.8516e-03	7.4940e-03
C_L/C_D	12.1855	13.2257
Λ_{LE}, deg	71.9–67.0	71.9–67.6
Aspect ratio	0.8701	0.9214
$(t/c)_{root,mid,tip}$, %	4.71, 3.07, 1.44	4.71, 2.32, 1.51
$(twst)_{root,mid,tip}$, deg	0.00, 0.50, 0.12	0.00, 0.50, 0.24
$\%A_{initial\ mid}$	68.7	52.0
$\%V_{initial\ wing}$	88.6	80.4

Table 7 Demographics from optimization cases[a]

	Coarse grid, 43 × 15 × 9	Fine grid, 127 × 43 × 25
Lift change, %	12.8	13.5
Drag change, %	−1.26	−2.22
C_L/C_D change, %	16.1	12.5
One-dimensional searches	69	88
Gradient evaluations	5	9
Memory, MWord	2.93	48.37
CPU time, h	0.53	38.1

[a]Direct sensitivity method [Eq. (8)] with ϑ(3) convergence.

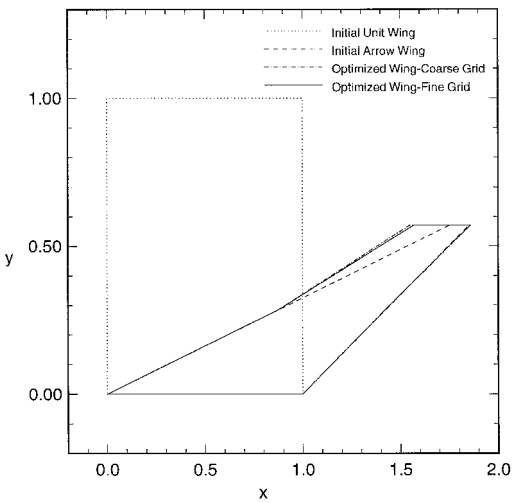

Fig. 6 Evolution of the wing–planform shape.

the maximization of C_L/C_D, subject to 14 geometric and two aerodynamic inequality constraints:

$$C_L \geq 0.11, \qquad C_D \leq 0.008$$
$$V_{wing} \geq 0.9V_{initial\ wing} \qquad A_{midspan} \geq 0.6A_{initial\ midspan} \tag{10}$$

At the root, mid, and tip sections:

$$2\ \text{deg} \leq \theta_{0.90\,chord} \leq 20\ \text{deg}, \qquad 2\ \text{deg} \leq \theta_{0.98\,chord} \leq 20\ \text{deg} \tag{11}$$

The volume constraint prevented the wing from becoming too thin, whereas the θ constraint ensures that the trailing edge does not become too sharp or too blunt. Also, side (equality) constraints were imposed on the design variables; for example, `spn` was tightly bound to avoid the optimizer seeking higher lift by simply increasing the wing span. The selected values of the design variables allowed for the formation of a planform break in the chord distribution. Also, the thickness, sweep, and geometrical twist were allowed to have linear spanwise distributions. The airfoil section at the wing root was elected to remain unchanged. For both of the cases, C_L, θ_{tip} at 90% chord, and V constraints were violated in the final design. Additionally, for the fine-grid optimization, $A_{midspan}$ constraint was also violated.

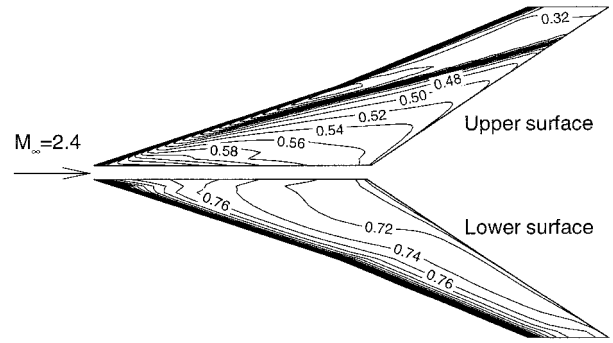

Fig. 7 Normalized pressure contours on optimized arrow wing obtained by ADI method on fine grid (127 × 43 × 25). M_∞ = 2.4, AOA = 3 deg.

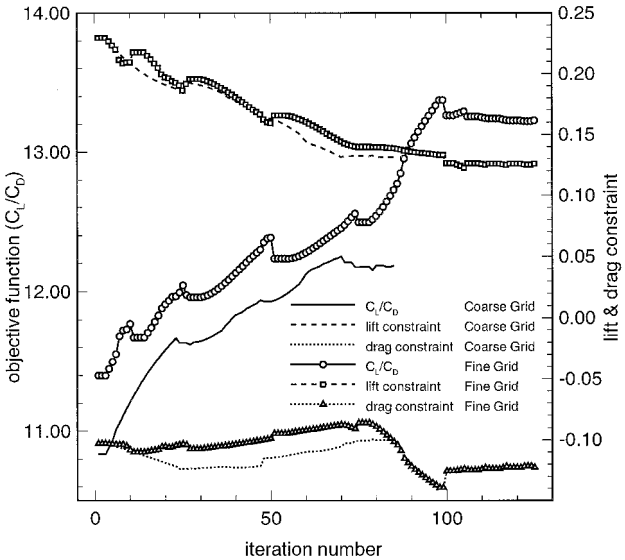

Fig. 8 Histories of objective function and aerodynamic constraints.

The optimization resulted in a cranked arrow wing (Figs. 5 and 6). The primary change was observed in the enlarged tip chord, the planform break, reduced thickness, and the increased geometric twist. A summary of the optimized wing's geometry and aerodynamics is given in Table 6 (for initial wing, see Tables 1 and 2). The surface pressures of the optimized wing are presented in Fig. 7, which may be contrasted with Fig. 4. The objective function histories during the evolution to the optimized shape are presented in Fig. 8. The trends appear similar for the coarse- and the fine-grid cases, but the values are distinctly different and the coarse-grid shape converged in fewer iterations. Finally, Table 7 presents some of the demographics for these optimization cases. It should be noted that the PCG method, had it been used for this fine-grid shape optimization, would require 164 MWord memory.

Conclusions

A gradient-based shape optimization methodology, which is intended for reasonably practical three-dimensional aerodynamic applications, has been developed. To accommodate the inherent larger size of such problems, the fluid dynamic and the aerodynamic sensitivity equations were solved using the ADI algorithm for memory efficiency.

The flow analysis for an arrow wing at Mach 2.4 compared well with those obtained using an unfactored approach (PCG), and an extensively used CFD code. The sensitivities of the present method have also compared well with those obtained using the PCG approach and finite difference approach. As expected, the ADI method reduced the storage memory but increased the computing time as compared to the PCG method. It should be mentioned that, although initial flowfield analysis for the PCG method appeared to be more time intensive as compared to the ADI method (Table 1), in a typical optimization cycle, two successive designs are only incrementally different, and this feature would be very much amenable for the efficacy of PCG to render CPU-time efficient designs. The new procedure has been demonstrated in the design of a cranked arrow wing. Effects of grid refinement and convergence tolerance on the analyses as well as the shape optimization results have been explored.

The results indicate that shape optimization problems that require large numbers of grid points can be resolved with a gradient-based approach. Therefore, to better utilize the computational resources, it is recommended that a number of coarse grid cases, using the PCG method, should initially be conducted to better define the optimization problem and the design space, and obtain an improved initial shape. Subsequently, a fine-grid shape optimization should be conducted using the ADI method to accurately obtain the final optimized shape.

Acknowledgments

This research was supported by NASA Langley Research Center under Grant NCC-1-211. The Technical Monitor was James L. Thomas.

References

[1]Hicks, R. M., and Henne, P. A., "Wing Design by Numerical Optimization," AIAA Paper 77-1247, Aug. 1977.

[2]Ibrahim, A. H., and Baysal, O., "Design Optimization Using Variational Methods and CFD," AIAA Paper 94-0093, Jan. 1994.

[3]Reuther, J., and Jameson, A., "Supersonic Wing and Wing-Body Shape Optimization Using an Adjoint Formulation," *CFD for Design and Optimization*, edited by O. Baysal, American Society of Mechanical Engineers, FED-Vol. 232, 1995, pp. 45–52.

[4]Baysal, O., and Eleshaky, M. E., "Aerodynamic Sensitivity Analysis Methods for the Compressible Euler Equations," *Journal of Fluids Engineering*, Vol. 113, No. 4, 1991, pp. 681–688.

[5]Huan, J., and Modi, V., "Design of Minimum Drag Bodies in Incompressible Laminar Flow," *CFD for Design and Optimization*, edited by O. Baysal, American Society of Mechanical Engineers, FED-Vol. 232, 1995, pp. 37–44.

[6]Baysal, O., and Eleshaky, M. E., "Aerodynamic Design Optimization Using Sensitivity Analysis and Computational Fluid Dynamics," *AIAA Journal*, Vol. 30, No. 3, 1992, pp. 718–725.

[7]Burgreen, G. W., Baysal, O., and Eleshaky, M. E., "Improving the Efficiency of Aerodynamic Shape Design Procedures," *AIAA Journal*, Vol. 32, No. 1, 1994, pp. 69–76.

[8]Burgreen, G. W., and Baysal, O., "Aerodynamic Shape Optimization Using Preconditioned Conjugate Gradient Methods," *AIAA Journal*, Vol. 32, No. 11, 1994, pp. 2145–2152.

[9]Eleshaky, M. E., and Baysal, O., "Aerodynamic Shape Optimization via Sensitivity Analysis on Decomposed Computational Domains," *Journal of Computers and Fluids*, Vol. 23, No. 4, 1994, pp. 595–611.

[10]Eleshaky, M. E., and Baysal, O., "Preconditioned Domain Decomposition Scheme for 3-D Aerodynamic Sensitivity Analysis," *AIAA Journal*, Vol. 32, No. 12, 1994, pp. 2489–2491.

[11]Eleshaky, M. E., and Baysal, O., "Design of 3-D Nacelle near Flat-Plate Wing Using Multiblock Sensitivity Analysis (ADOS)," AIAA Paper 94-0160, Jan. 1994.

[12]Beam, R. M., and Warming, R. F., "An Implicit Factored Scheme for the Compressible Navier-Stokes Equations," *AIAA Journal*, Vol. 16, No. 4, 1978, pp. 393–402.

[13]Korivi, V. M., Taylor, A. C., III, Hou, G. W., Newman, P. A., and Jones, H. E., "Sensitivity Derivatives for Three-Dimensional Supersonic Euler Code Using Incremental Iterative Strategy," *AIAA Journal*, Vol. 32, No. 6, 1994, pp. 1319–1321.

[14]Burgreen, G. W., and Baysal, O., "3-D Aerodynamic Shape Optimization Using Discrete Sensitivity Analysis," *AIAA Journal*, Vol. 34, No. 9, 1996, pp. 1761–1770.

[15]Burgreen, G. W., and Baysal, O., "Three-Dimensional Aerodynamic Shape Optimization of Delta Wings," *Proceedings of the AIAA/USAF/NASA/ISSMO 5th Multidisciplinary Analysis and Optimization Conference* (Panama City, FL), AIAA, Washington, DC, 1994, pp. 87–97.

[16]Narducci, R., Grossman, B., Valorani, M., Dadone, A., and Haftka, R. T., "Optimization Methods for Non-Smooth or Noisy Objective Functions in Fluid Design Problems," *Proceedings of the AIAA 12th Computational Fluid Dynamics Conference* (San Diego, CA), AIAA, Washington, DC, 1995, pp. 21–32.

[17]Vanderplaats, G. N., "ADS — A FORTRAN Program for Automated Design Synthesis — Version 1.10," NASA CR 177985, Sept. 1985.

[18]Thomas, J. L., Krist, S. T., and Anderson, W. K., "Navier-Stokes Computations of Low Aspect Ratio Wings," *AIAA Journal*, Vol. 28, No. 2, 1990, pp. 205–215.